HOKKAIDO UNIVERSITY

Title	Effects of vacuum annealing on the electron mobility of epitaxial La-doped BaSnO3 films
Author(s)	Cho, Hai Jun; Onozato, Takaki; Wei, Mian; Sanchela, Anup; Ohta, Hiromichi
Citation	APL materials, 7(2), 022507 https://doi.org/10.1063/1.5054154
Issue Date	2019-02
Doc URL	http://hdl.handle.net/2115/75115
Rights	© 2019 Hai Jun Cho, Takaki Onozato, Mian Wei, Anup Sanchela, and Hiromichi Ohta
Rights(URL)	https://creativecommons.org/licenses/by/4.0/
Type	article
File Information	1.5054154.pdf

Instructions for use

Hokkaido University Collection of Scholarly and Academic Papers : HUSCAP

APL Materials

Effects of vacuum annealing on the electron mobility of epitaxial La-doped $BaSnO_3$ films

Cite as: APL Mater. **7**, 022507 (2019); https://doi.org/10.1063/1.5054154
Submitted: 30 August 2018 . Accepted: 31 October 2018 . Published Online: 12 December 2018

Hai Jun Cho, Takaki Onozato, Mian Wei, Anup Sanchela, and Hiromichi Ohta

ARTICLES YOU MAY BE INTERESTED IN

Epitaxial integration of high-mobility La-doped $BaSnO_3$ thin films with silicon
APL Materials **7**, 022520 (2019); https://doi.org/10.1063/1.5054810

Large thickness dependence of the carrier mobility in a transparent oxide semiconductor, La-doped $BaSnO_3$
Applied Physics Letters **112**, 232102 (2018); https://doi.org/10.1063/1.5033326

Thin-film stabilization of $LiNbO_3$-type $ZnSnO_3$ and $MgSnO_3$ by molecular-beam epitaxy
APL Materials **7**, 022505 (2019); https://doi.org/10.1063/1.5054289

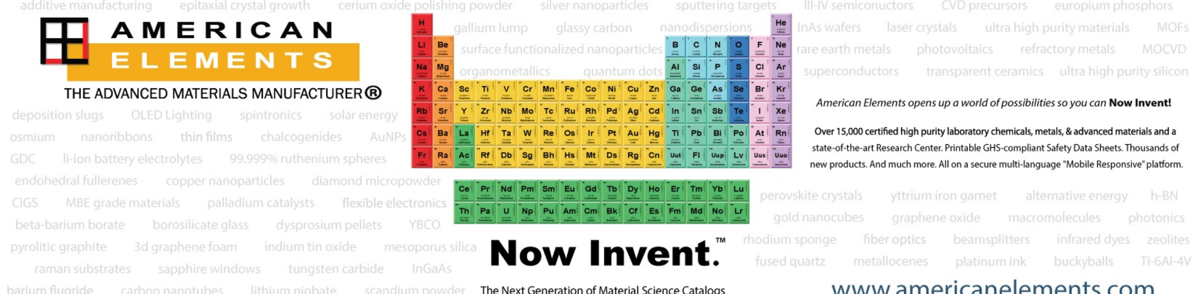

© 2018 Author(s).

Effects of vacuum annealing on the electron mobility of epitaxial La-doped $BaSnO_3$ films

Cite as: APL Mater. 7, 022507 (2019); doi: 10.1063/1.5054154
Submitted: 30 August 2018 • Accepted: 31 October 2018 •
Published Online: 12 December 2018

View Online

Export Citation

CrossMark

Hai Jun Cho,[1,2,a)] Takaki Onozato,[2] Mian Wei,[2] Anup Sanchela,[1] and Hiromichi Ohta[1,2,a)]

AFFILIATIONS

[1] Research Institute for Electronic Science, Hokkaido University, N20W10, Kita, Sapporo 001-0020, Japan
[2] Graduate School of Information Science and Technology, Hokkaido University, N14W9, Kita, Sapporo 060-0814, Japan

[a)] Authors to whom correspondence should be addressed: joon@es.hokudai.ac.jp and hiromichi.ohta@es.hokudai.ac.jp

ABSTRACT

Wide bandgap (E_g ~ 3.1 eV) La-doped $BaSnO_3$ (LBSO) has attracted increasing attention as one of the transparent oxide semiconductors since its bulk single crystal shows a high carrier mobility (~320 cm^2 V^{-1} s^{-1}) with a high carrier concentration (~10^{20} cm^{-3}). For this reason, many researchers have fabricated LBSO epitaxial films thus far, but the obtainable carrier mobility is substantially low compared to that of single crystals due to the formation of the lattice/structural defects. Here we report that the mobility suppression in LBSO films can be lifted by a simple vacuum annealing process. The oxygen vacancies generated from vacuum annealing reduced the thermal stability of LBSO films on MgO substrates, which increased their carrier concentrations and lateral grain sizes at elevated temperatures. As a result, the carrier mobilities were greatly improved, which does not occur after heat treatment in air. We report a factorial design experiment for the vacuum annealing of LBSO films on MgO substrates and discuss the implications of the results. Our findings expand our current knowledge on the point defect formation in epitaxial LBSO films and show that vacuum annealing is a powerful tool for enhancing the mobility values of LBSO films.

© 2018 Author(s). All article content, except where otherwise noted, is licensed under a Creative Commons Attribution (CC BY) license (http://creativecommons.org/licenses/by/4.0/). https://doi.org/10.1063/1.5054154

Transparent oxide semiconductors (TOSs) are promising candidates for various future electronic devices such as transistors, solar cells, and display panels.[1,2] For such applications, high electron mobility (μ) is essential, and this has been a great disadvantage for TOS materials since their mobility values are low compared to classical semiconductors. In this regard, perovskite La-doped $BaSnO_3$ (LBSO) is gaining significant interest since its bulk single crystal exhibits a wide bandgap (~3.1 eV) and a very high mobility of 320 cm^2 V^{-1} s^{-1},[3,4] which is comparable to that of doped single crystal Si (~350 cm^2 V^{-1} s^{-1}).[5] For this reason, there have been many attempts to utilize LBSO in thin films transistors.

However, crystalline defects prevent the μ in LBSO films from reaching the single crystal value, and many studies were devoted to improving the crystal quality of epitaxial LBSO films.[6–12] For example, since misfit dislocations occur at the film/substrate interface due to the lattice mismatch, buffer layers are commonly used to reduce the dislocations.[13,14] To completely eliminate the film/substrate mismatch, Lee *et al.* grew LBSO films on single crystal $BaSnO_3$ substrate.[15] In addition, in our recent study, we fabricated LBSO films under an ozone atmosphere to reduce the amount of point defects.[16] Unfortunately, while these approaches were successful in improving the mobility values in LBSO films (up to ~120 cm^2 V^{-1} s^{-1}), they can significantly increase the fabrication cost, which may be a crucial issue in mass production systems at industrial scales.

In large scale production facilities, designing a clever post treating process is often more economical than improving the quality of as-deposited samples. In this regard, very interesting experimental results were released in 2015 and 2018. In one study, N_2 environment at 1000 °C was used to create oxygen vacancies in the LBSO films on $SrTiO_3$ substrates, and the μ increased from 41 cm^2 V^{-1} s^{-1} to 78 cm^2 V^{-1} s^{-1}.[17] In the other study (same research group), oxygen vacancies were generated in the LBSO films on $SrTiO_3$ substrates using H_2

© Author(s) 2018

forming gas at 950 °C, which further improved the μ up to 122 cm^2 V^{-1} s^{-1}.[18] According to these studies, oxygen vacancies can neutralize the negative charges at threading dislocations[19–21] and induce lateral grain growth at elevated temperatures.

As removing oxygen ions (O^{2-}) near threading dislocations decreases their thermal stability, oxygen vacancy doping creates a very strong driving force for lateral grain growths at high temperatures, which significantly increases the free propagation length of the carrier electrons. These results suggest that post treating of LBSO films can be just as effective as modifying the synthesis methods for improving the as-deposited crystal quality of LBSO films. In undoped $BaSnO_3$ films, vacuum annealing is commonly used to create oxygen vacancies and induce mobile charge carriers.[22,23] Since vacuum annealing process is much simpler than creating N_2 or H_2 forming gas environment, it can be an alternative method for inducing oxygen vacancy assisted grain growths in LBSO films. In addition, since the deposition of oxide takes place in a vacuum chamber, the film growth and post annealing can be combined into one process. There is one study that examined the effect of vacuum annealing on the electron transport properties of LBSO films,[24] but the reported μ values are too low (<4 cm^2 V^{-1} s^{-1}) to validate vacuum annealing as an effective method for improving μ.

For optimizing the post annealing process, it is important to understand point defect formation in LBSO films because the μ-enhancement in LBSO films begins from generating oxygen vacancies. In stoichiometric $BaSnO_3$, the oxidation states of its constituents are Ba^{2+} = [Xe], Sn^{4+} = [Kr] $4d^{10}$, and O^{2-} = [Ne]. Since two of the constituents (Ba^{2+}, O^{2-}) exhibit the same orbitals with inert gases (Xe, Ne), stoichiometric $BaSnO_3$ crystals are believed to be thermodynamically stable,[25] and stoichiometric $BaSnO_3$ films do not intrinsically conduct electricity as all electrons form firmly bound states. The formation energy of oxygen vacancy in $BaSnO_3$ is high and can only be lowered by reducing the chemical potential of oxygen,[26] which can be achieved by lowering oxygen pressure during the film growth[27,28] or vacuum annealing at high temperatures.[22,23] Therefore, as-deposited $BaSnO_3$ films do not have sufficient oxygen vacancies to conduct electricity unless they are intentionally created. By contrast, oxygen vacancies are much more common in LBSO films even if sufficient oxygen is provided during the film growth.[18] In one of our previous studies, Sn^{2+} states were detected from LBSO films fabricated under 10 Pa of O_2, which implies the presence of oxygen deficiency.[16,27] These results suggest that the La-dopants may be promoting oxygen vacancy formations in $BaSnO_3$ films. However, the relationship between La-dopants and oxygen vacancy in $BaSnO_3$ has not been investigated in detail.

In this study, we studied the effect of La-dopants on the formation of oxygen vacancy in LBSO films and investigated the feasibility of enhancing the μ of LBSO films using vacuum annealing. According to our results, vacuum annealing significantly increases the μ of LBSO films. We also found that La-dopants increased the oxygen vacancy vs. lattice oxygen (V_O/L_O) ratio in as-deposited LBSO films and affected the vacuum annealing effect. The results of this study expand our current knowledge on the point defect formation in epitaxial LBSO films and show that vacuum annealing is a simple and effective method for enhancing the electron mobility of LBSO films.

LBSO epitaxial films ([La^{3+}] = 0.1%, 0.55%, 1%, 2%, 5%, and 7%) were fabricated on (001)-oriented MgO substrates at 750 °C using pulsed laser deposition (PLD, KrF excimer laser, fluence ~2 J cm^{-2} $pulse^{-1}$, repetition rate = 10 Hz). The oxygen pressure inside the chamber during the film growth was kept at 10 Pa. High-resolution X-ray diffraction (XRD, Cu $K\alpha_1$, ATX-G, Rigaku Co.) and reciprocal space mappings (RSMs) were performed around (204) diffraction spots of the LBSO films. Using Scherrer's equation, the lateral grain sizes of the LBSO were estimated with the reciprocal space mappings (RSMs) diffraction spot widths (Fig. 1). The film thicknesses were measured from the Kiessig or Pendellöesung fringes in the XRD patterns (data not shown). The electrical conductivity (σ), carrier concentration (n), and Hall mobility (μ_{Hall}) of the films were measured at room temperature by the conventional dc 4-probe method in the van der Pauw electrode geometry.

To confirm that vacuum annealing can induce grain growth in LBSO films, a 2% LBSO film (~64 nm) was prepared and cut it into two pieces. We annealed one piece in air and the other piece in vacuum (<10^{-2} Pa) at 750 °C for 1 h. Then, we measured the lateral grain sizes of the films before and after the heat treatments using the RSM (Fig. 1). While the (204) diffraction spot of the air annealed film was almost the same with that of the as-deposited film, the (204) diffraction spot of the vacuum annealed was two times more intense compared to the other two films (as-deposited and air-annealed). The lateral grain sizes (D) of the as-deposited, air annealed, and vacuum annealed LBSO films were 9.1 nm, 10.2 nm, and 22.3 nm, respectively. The small grain size change after air annealing is not surprising since the film was deposited at 750 °C, and no significant change in the microstructure was expected. On the other hand, the vacuum annealing substantially increased the lateral grain size, which is consistent with the H_2 forming gas experiment.[18] This shows that vacuum annealing can indeed be an alternative method for triggering oxygen vacancy assisted grain growth in LBSO films.

In order to find the optimum vacuum annealing temperature, several 2% LBSO films with similar thicknesses (~41 nm) and electrical properties were fabricated (supplementary Table S1), and they were annealed in vacuum (<10^{-2} Pa) at different temperatures ranging from 650 °C to 800 °C for 30 min. With increasing annealing temperature, the D of the films increased gradually from ~5 nm to ~17 nm [Fig. 2(a) and supplementary Fig. S1]. Figures 2(b) and 2(c) summarize the effect of the vacuum annealing on the electron transport properties of the LBSO film. The n increased from ~1.35×10^{20} cm^{-3} up to ~1.8×10^{20} cm^{-3} when the sample

© Author(s) 2018

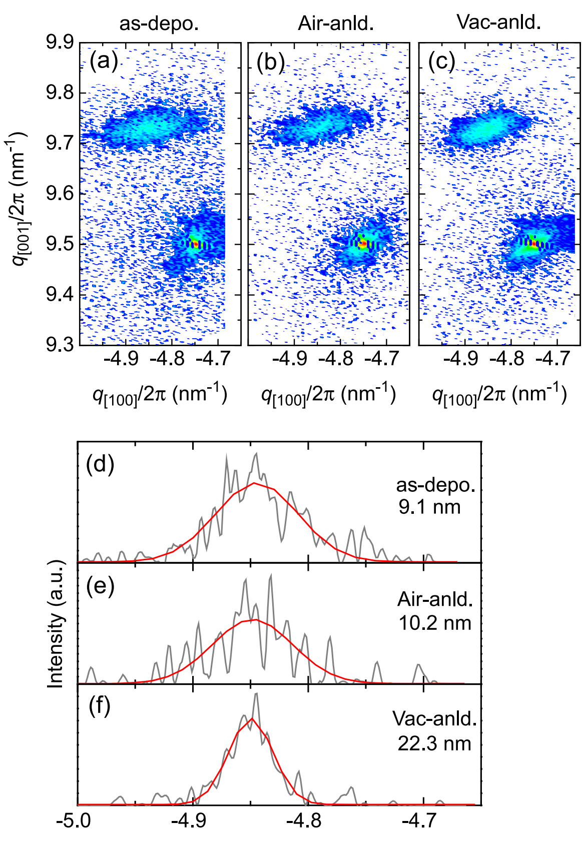

FIG. 1. Lateral grain growth of the LBSO film by the vacuum annealing. [(a)–(c)] RSMs near (204) diffraction peak of 2% La-doped LBSO films (~64 nm) [(a) as-deposited film, (b) air-annealed at 750 °C for 1 h, and (c) vacuum annealed at 750 °C for 1 h]. The RSMs were shifted using the peak position of (204) MgO ($q_{[100]}/2\pi$ = 9.50 nm^{-1}, $q_{[100]}/2\pi$ = –4.75 nm^{-1}). [(d)–(f)] Diffraction spots of the LBSO films along the *x*-axis in the RSM. The lateral grain sizes (*D*) of the films are inversely proportional to the integral width. The *D* values extracted from the RSMs were (a) and (d) 9.1 nm, (b) and (e) 10.2 nm, and (c) and (f) 22.3 nm, respectively. The as-deposited film was cut into two pieces. One was annealed in air, while the other was annealed in vacuum. Almost no change in the RSM was observed from air-annealing. On the other hand, significant increase in the lateral grain size and peak intensity can be noticed from the vacuum annealed film. Unfortunately, electrical properties of the annealed samples could not be measured since they were cut from a 1 cm^2 square sample, and our probe station can only measure 1 cm^2 square coupons.

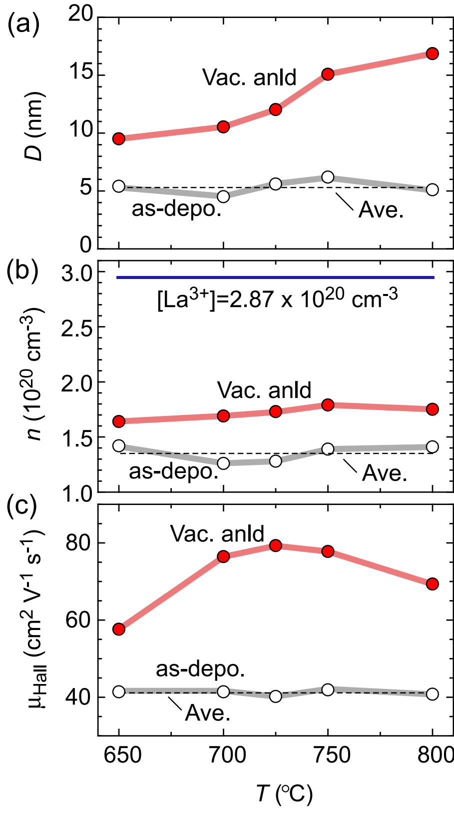

FIG. 2. Optimum vacuum annealing temperature for the 2% La-doped LBSO film. (a) Lateral grain size (*D*) increased gradually with vacuum (<10^{-2} Pa) annealing temperature. (b) The carrier concentration (*n*) increased from ~1.35 × 10^{20} cm^{-3} to ~1.8 × 10^{20} cm^{-3} when the sample was annealed in the vacuum. The observed *n* is lower than [La^{3+}] (=2.87 × 10^{20} cm^{-3}), indicating the activation of La^{3+} is low. (c) The Hall mobility (μ_{Hall}) greatly increased with temperature when the sample was annealed in the vacuum up to ~80 cm^2 V^{-1} s^{-1} from the as-deposited mobility of ~40 cm^2 V^{-1} s^{-1}. The optimum vacuum annealing temperature turned out to be 725 °C.

was annealed in the vacuum [Fig. 2(b)]. The observed n was far lower than the [La^{3+}] (=2.87 × 10^{20} cm^{-3}), indicating the low carrier activation rate of the La^{3+} ions. The μ_{Hall} of the films greatly increased (up to ~80 cm^2 V^{-1} s^{-1}) after vacuum annealing. The highest μ_{Hall} was observed from the LBSO film vacuum annealed at 725 °C [Fig. 2(c)]. Above 725 °C, the μ_{Hall} started to decrease despite the increase in the D. This is likely attributed to high oxygen vacancy generation rate or chemical reaction at elevated temperatures. According to this result, 725 °C is the optimal vacuum annealing temperature for LBSO films on MgO substrates. Once the films became thicker than ~120 nm, both the as-deposited and vacuum annealed mobility values saturated at ~84 cm^2 V^{-1} s^{-1} and ~100 cm^2 V^{-1} s^{-1}, respectively. Both as-deposited and vacuum annealed D exhibited strong thickness dependence (supplementary Fig. S2a). We believe the grain growth is hindered by the lattice strain, which decreases with increasing thickness.[29] The highest mobility observed was 101.6 cm^2 V^{-1} s^{-1} from vacuum annealed 117 nm LBSO film (as deposited: ~74 cm^2 V^{-1} s^{-1}, supplementary Fig. S2d), which is comparable to that observed in LBSO films with buffer layers. This confirms that vacuum annealing is an effective method for enhancing the mobility of LBSO films.

To find the effect of La-dopants on the vacuum annealing process, we annealed LBSO films (average thickness: 43 nm) with varying [La^{3+}] at 725 °C in vacuum for 30 min. Figure 3 summarizes the electron transport properties of the annealed LBSO films. The n of the LBSO films always showed an increase

© Author(s) 2018

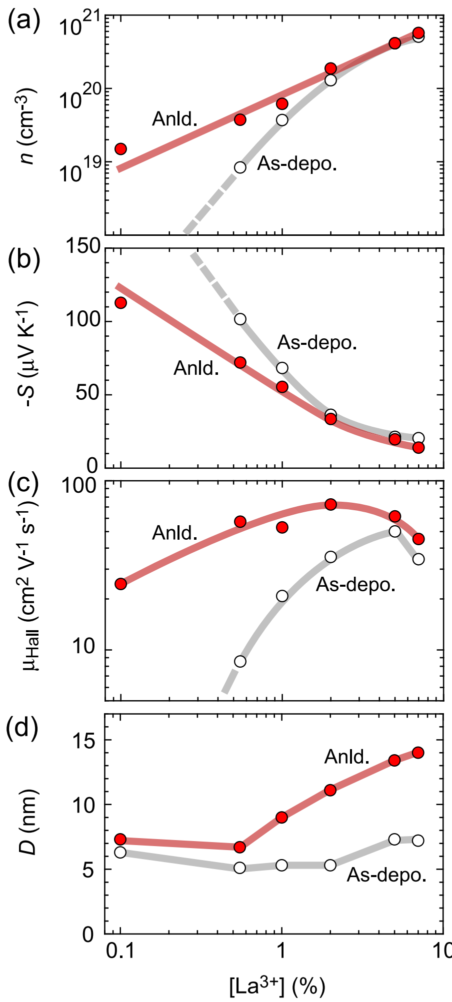

FIG. 3. La-concentration dependences of the electron transport properties and the lateral grain size for the vacuum annealed LBSO films (725 °C, <10^{-2} Pa, 30 min). (a) Carrier concentration (n) of the vacuum annealed LBSO films shows linearly increases with [La^{3+}] while the as-deposited LBSO films show lower n. (b) The absolute value of thermopower (S) decreases with [La^{3+}], which reflects n *vs* [La^{3+}] relation.[30] (c) The Hall mobility (μ_{Hall}) of the annealed LBSO films was dramatically enhanced at low [La^{3+}] compared with the as-deposited LBSO films. (d) Lateral grain size (D) of the LBSO films before and after vacuum annealing. D for the annealed samples increased when [La^{3+}] is greater than 1%.

with [La^{3+}] while the vacuum annealed films exhibited higher n compared to the as-deposited films [Fig. 3(a)]. The 0.1% LBSO film, which did not conduct electricity, also became electrically conductive. The absolute value of thermopower (S) decreased with [La^{3+}], which reflects the relationship between n and [La^{3+}] [Fig. 3(b)].[30] The μ_{Hall} of the annealed LBSO films was dramatically improved compared with the as-deposited LBSO films [Fig. 3(c)], but the lateral grain size enhancement exhibited a strong doping dependence. At low doping levels (≤0.55%), the grain sizes did not increase much after vacuum annealing. The grain size change became noticeable from 1% [La^{3+}] and saturated at 2% [La^{3+}] [Fig. 3(d)]. Interestingly, while the highest as-deposited μ_{Hall} was observed in the 5% LBSO film, the highest μ_{Hall} after vacuum annealing was observed in the 2% LBSO film (35.5 cm^2 V^{-1} s^{-1} → 72.3 cm^2 V^{-1} s^{-1}) although the annealed lateral grain size was highest in 7% LBSO film. The decrease in the vacuum annealed mobility from the 5% film is attributed to impurity scatterings from La dopants themselves. This suggests that impurity scatterings start to become significant if the lateral grain size is greater than ~12 nm [Figs. 3(c) and 3(d)]. These results indicate that 2% LBSO films have an optimized balance between oxygen vacancy formation, impurity scattering (μ_{Hall} ↓), and oxygen vacancy induced grain growth (μ_{Hall} ↑) for vacuum heat treatments.

It is important to note that mobility improvements were observed from 0.1% to 0.55% LBSO films despite the small changes in their grain sizes. In epitaxial films, threading dislocations often exhibit negative charges and generate energy barriers (mobility edge).[19–21] Therefore, mobilities in epitaxial films can depend on the Fermi energy (E_F), which increases with the carrier concentration. Since vacuum annealing increases both n and D, the μ_{Hall} improvements observed from 0.1% to 0.55% are mainly attributed to the E_F shift from additional charge carriers because they did not show significant grain size changes. This also implies that mobility improvements observed at other doping levels could have been affected the increase in n (i.e., higher E_F). To confirm the effect of E_F shift on μ_{Hall}, we vacuum annealed a 2% LBSO (45.7 nm) film from 100 °C to 800 °C in sequence in steps of 100 °C (i.e., vac. anneal 100 °C → 200 °C →···→ 800 °C) to generate additional charge carriers while minimizing the grain growth. During the sequence annealing, the carrier concentration of the film gradually increased, but its electron mobility remained almost unchanged (supplementary Fig. S5). The drastic drop in μ_{Hall} at 800 °C is likely from structural damages due to high V_O generation rate. The sequence annealing shows that the E_F at $n \sim 0.5 \times 10^{20}$ cm^{-3} exceeds the mobility edge of the LBSO films on MgO substrates, and the vacuum annealed mobilities are not strongly affected by the Fermi energy shift if $n > 0.5 \times 10^{20}$ cm^{-3}. This number is consistent with the H_2 forming gas experiment, where two post-treated LBSO films with the same carrier concentration of 1.1×10^{20} cm^{-3} exhibited different mobility values due to structural differences.[18] According to our results, μ at low doping levels (0.1% and 0.55%) is dominated by the Fermi level. If $n > 0.5 \times 10^{20}$ cm^{-3}, the Fermi level seems to be above the mobility edge, and μ is mainly affected by electron scatterings (supplementary Fig. S5). The sources of electron scattering are point defects (impurity, V_O) and grain boundary (threading dislocation). The vacuum annealing effects observed from 2% to 5% LBSO films suggest that grain boundary scattering dominates up to $D \sim 12$ nm and point defect scattering dominates from $D > 12$ nm [Figs. 3(c) and 3(d)]. Therefore, majority of the mobility enhancement observed in 2% LBSO films (optimized doping) is attributed to the change in D because their E_F ($n > 1.0 \times 10^{20}$ cm^{-3}) are likely above the mobility edge.

In order to further investigate the effect of the vacuum annealing on the μ improvement of the LBSO films,

© Author(s) 2018

we performed the X-ray photoelectron spectroscopy (XPS) measurement of the LBSO films [Fig. 4(a): as-deposited, Fig. 4(b): vacuum annealed]. In case of oxygen in perovskite oxides, the lattice oxygen peak (L_O) is located at ~529 eV. If oxygen vacancies are present, this peak shifts to ~531 eV (V_O).[18,31,32] Another oxygen peak around 532 ~ 533 eV (A_O) can emerge from chemically adsorbed oxygen from surface contamination by organic molecules. The source of chemically adsorbed oxygen is unknown, but we believe it is related to the status of the vacuum chambers (annealing, XPS) or storing conditions. For the XPS peak fitting, a convolution between Gaussian (70%) and Lorentzian (30%) was used. For each LBSO films, the full width at half maximum (FWHM) was constrained to be the same for all 3 oxygen peaks.

The V_O peak energies of the LBSO films increased after vacuum annealing, especially for films with higher [La^{3+}] [Fig. 4(c)]. The V_O/L_O area ratio from the XPS of the as-deposited LBSO films increased gradually when the [La^{3+}] exceeded 1% (supplementary Table S2). Upon vacuum annealing, this ratio increased further for all films except for 7% LBSO film. The largest change in V_O/L_O was observed from 2% doped LBSO film. Since the solubility limit of La in LBSO was reported to be ~5%, the oxygen vacancy reduction in 7% LBSO is likely attributed to the formation of $La_2Sn_2O_7$,[33] which could be observed from the ceramic targets used to deposit the films (supplementary Fig. S6). These results show that La-dopants in epitaxial LBSO films affect not only the oxygen stability but also the thermal stability of the film.

The XPS results show that vacuum annealing increases oxygen deficiency in the LBSO films, and oxygen vacancies in oxides normally provide additional conduction electrons. However, associating all changes in n to additional V_O from vacuum annealing does not adequately explain our results. For example, according to the thickness dependence, the carrier concentration enhancement was greatly reduced with increasing thickness [Fig. 2(c)] although the oxygen vacancy generated from vacuum annealing would have been similar as the La^{3+} doping levels were the same unless the chemical potential of oxygen depends on the lattice strain. In addition, in the [La^{3+}] dependence, the changes in n [Fig. 3(a)] do not match the changes in V_O/L_O [Fig. 4(c)]. The implications of these phenomena can be very interesting as they suggest strain-dependent oxygen stability or oxygen vacancies not generating additional charge carriers. However, no firm conclusions can be drawn at this moment since the vacuum annealing effect on the activation of [La^{3+}] dopant is unclear.

Although we demonstrated that the mobility boost in the optimally doped films (2%) after vacuum annealing is strongly related to the lateral grain sizes, we would like to note that there were a couple unusual instances. In supplementary Figs. S2(a) and S2(d), μ_{Hall} of vacuum annealed 280 nm film is slightly smaller than that of vacuum annealed 117 nm film although their grain sizes are both >12 nm and their electron densities are similar (2.2×10^{20} cm^{-3} and 2.1×10^{20} cm^{-3}). This is another indicator that suggests strain-dependent oxygen vacancy generation, but this hypothesis requires more experimental evidence. Furthermore, in Fig. 2, the LBSO films

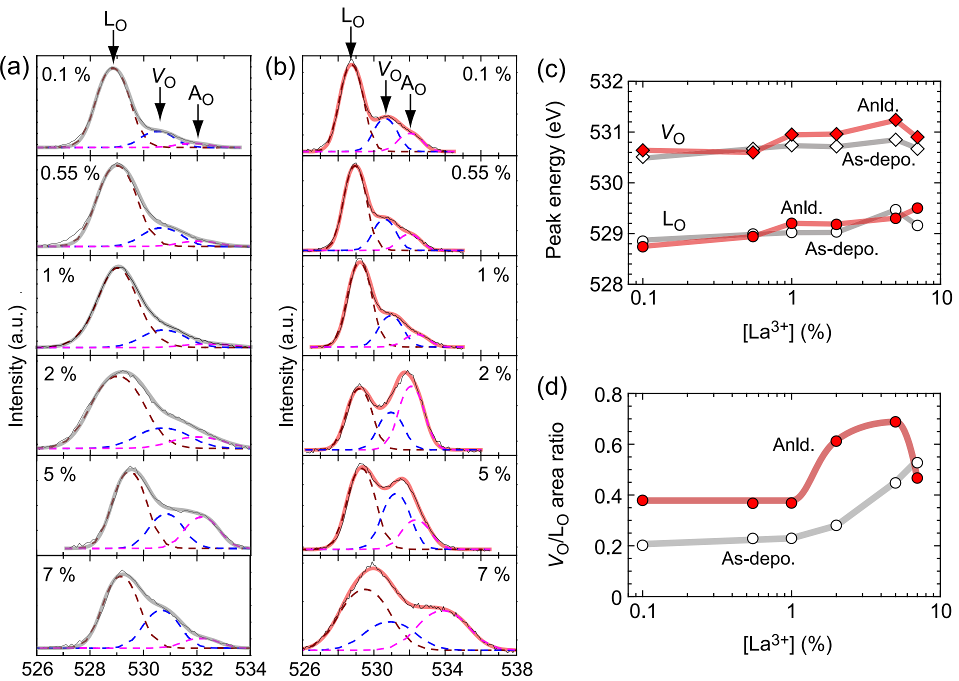

FIG. 4. Oxygen vacancy evolution in the LBSO films after the vacuum annealing. XPS spectra of the LBSO films at (a) the as-deposited states and (b) after the vacuum annealed states. The XPS peaks were decomposed into three peaks [L_O: Lattice oxygen (~529 eV), V_O: Oxygen vacancy (~531 eV), and A_O: chemically adsorbed oxygen (~532 eV)]. (c) Peak energies of L_O and V_O at different [La^{3+}]. The V_O at higher [La^{3+}] of the annealed sample locates higher energies as compared with that of as-deposited samples. (d) V_O/L_O area ratio, which was extracted from the XPS data. The V_O/L_O ratio in the as-deposited LBSO films increases gradually when the [La^{3+}] exceed 1%. The V_O/L_O ratio in the annealed LBSO films is almost double as compared with the as-deposited LBSO films.

© Author(s) 2018

vacuum annealed at 650 °C and 700 °C exhibit different mobility values despite having similar grain sizes and electron densities (Fig. 2). We believe these phenomena are related to the combination of all processes induced by vacuum annealing: increase in the carrier concentration, increase in the oxygen vacancy, and lateral grain growth. While these data make our study not perfect, we believe these results are still valuable as they emphasize the necessity and importance of understanding oxygen vacancy in LBSO films.

Finally, the role of La-dopants in the oxygen vacancy formation mechanism in the as-deposited LBSO films is also vague [Fig. 4(c)]. In this regard, we believe that the role of threading dislocation in point defect formation is important. For example, in case of unintentionally V_O doped $BaSnO_{3-\delta}$ single crystal, vacuum annealing reduces the carrier concentration and therefore reduces the oxygen vacancy level.[34] This contradicts the behavior of epitaxial $BaSnO_3$ films, where vacuum annealing increases the carrier concentration.[22,23] Since the main structural difference between single crystals and epitaxial films is the presence of threading dislocations, it is plausible to think that they can promote point defect formation in epitaxial films. In the context of this research, since impurities often segregate between grains separated by dislocations,[35] one possibility is the segregation of La-dopants at threading dislocations, which is plausible since La^{3+} ions can compensate the missing cationic charges at threading dislocations.[19–21] This scenario also explains the low dopant carrier activation rate observed in epitaxial LBSO films [Fig. 2(a)]. In this case, La^{3+} vacant sites in the grain interior may lose adjacent O^{2-} ions due to the lack of bonding electrons, but more work is required to confirm the role of threading dislocations as well as the activation of $[La^{3+}]$ dopants. Furthermore, it will be very interesting to re-anneal the vacuum annealed LBSO films in ambient air to inject oxygen back and fill oxygen vacancies. Unfortunately, although MgO has excellent vacuum stability, its thermal stability in air is poor,[36–38] and such experiments could not be considered in this study. However, annihilation of oxygen vacancies in the vacuum annealed films could potentially reduce defect scattering and further enhance the electron mobility.

In summary, we examined the effect of vacuum annealing on the electron transport properties of the epitaxial LBSO films on (001) MgO substrates. Lateral grain sizes and carrier concentrations of the LBSO films substantially increased after vacuum annealing whereas it remained almost unchanged after air annealing. We also found the oxygen vacancy vs. lattice oxygen (V_O/L_O) ratio in the XPS O 1s spectra increases with vacuum annealing, proving that oxygen vacancy generation indeed provides the driving force for this process. The results of this study clearly show that vacuum annealing improves electron mobility of LBSO films, where the mechanisms vary from Fermi energy shift to oxygen-vacancy-assisted-grain-growth depending on the doping levels. Unfortunately, we were not able to explain all observed phenomena in detail, but our results do highlight the necessity for more studies on the thermodynamic processes involved with vacuum annealing of epitaxial LBSO films.

The vacuum annealing approach was very effective for films with small thicknesses. Therefore, it is a very good method for making LBSO film transistors since low thicknesses are desired for reducing the power consumption. We believe these results will be useful for designing low cost fabrication methods for high-mobility LBSO films or can be used to improve the carrier mobility of other perovskite stannates such as $SrSnO_3$.

See supplementary material for detailed XPS characteristics and RSM patterns of the LBSO films.

We would like to thank the Hokkaido University Office for the Promotion of Nanotechnology Collaborative Research (Nanotechnology Platform) for their assistance. This research was supported by Grants-in-Aid for Scientific Research A (No. 17H01314) from JSPS, the Asahi Glass Foundation, and the Mitsubishi Foundation. A part of this work was supported by Dynamic Alliance for Open Innovation Bridging Human, Environment and Materials as well as the Network Joint Research Center for Materials and Devices. Student aids from JSPS (T. Onozato, No. 17J01281) and China Scholarship Council (M. Wei) are also greatly appreciated.

REFERENCES

[1] D. Ginley, H. Hosono, and D. C. Paine, *Handbook of Transparent Conductors* (Springer, 2011).
[2] P. Barquinha, R. Martins, L. Pereira, and E. Fortunato, *Transparent Oxide Electronics: From Materials to Devices* (Wiley, 2012).
[3] H. J. Kim, U. Kim, H. M. Kim, T. H. Kim, H. S. Mun, B. G. Jeon, K. T. Hong, W. J. Lee, C. Ju, K. H. Kim, and K. Char, Appl. Phys. Express **5**, 061102 (2012).
[4] H. J. Kim, U. Kim, T. H. Kim, J. Kim, H. M. Kim, B. G. Jeon, W. J. Lee, H. S. Mun, K. T. Hong, J. Yu, K. Char, and K. H. Kim, Phys. Rev. B **86**, 165205 (2012).
[5] N. M. Johnson, C. Herring, and D. J. Chadi, Phys. Rev. Lett. **56**, 769 (1986).
[6] H. Paik, Z. Chen, E. Lochocki, H. A. Seidner, A. Verma, N. Tanen, J. Park, M. Uchida, S. L. Shang, B. C. Zhou, M. Brutzam, R. Uecker, Z. K. Liu, D. Jena, K. M. Shen, D. A. Muller, and D. G. Schlom, APL Mater. **5**, 116107 (2017).
[7] S. Raghavan, T. Schumann, H. Kim, J. Y. Zhang, T. A. Cain, and S. Stemmer, APL Mater. **4**, 016106 (2016).
[8] Z. Lebens-Higgins, D. O. Scanlon, H. Paik, S. Sallis, Y. Nie, M. Uchida, N. F. Quackenbush, M. J. Wahila, G. E. Sterbinsky, D. A. Arena, J. C. Woicik, D. G. Schlom, and L. F. J. Piper, Phys. Rev. Lett. **116**, 027602 (2016).
[9] P. V. Wadekar, J. Alaria, M. O'Sullivan, N. L. O. Flack, T. D. Manning, L. J. Phillips, K. Durose, O. Lozano, S. Lucas, J. B. Claridge, and M. J. Rosseinsky, Appl. Phys. Lett. **105**, 052104 (2014).
[10] C. A. Niedermeier, S. Rhode, S. Fearn, K. Ide, M. A. Moram, H. Hiramatsu, H. Hosono, and T. Kamiya, Appl. Phys. Lett. **108**, 172101 (2016).
[11] U. Kim, C. Park, T. Ha, R. Kim, H. S. Mun, H. M. Kim, H. J. Kim, T. H. Kim, N. Kim, J. Yu, K. H. Kim, J. H. Kim, and K. Char, APL Mater. **2**, 056107 (2014).
[12] H. Mun, U. Kim, H. M. Kim, C. Park, T. H. Kim, H. J. Kim, K. H. Kim, and K. Char, Appl. Phys. Lett. **102**, 252105 (2013).
[13] J. Shiogai, K. Nishihara, K. Sato, and A. Tsukazaki, AIP Adv. **6**, 065305 (2016).
[14] A. Prakash, P. Xu, A. Faghaninia, S. Shukla, J. W. Ager, C. S. Lo, and B. Jalan, Nat. Commun. **8**, 15167 (2017).
[15] W. J. Lee, H. J. Kim, E. Sohn, T. H. Kim, J. Y. Park, W. Park, H. Jeong, T. Lee, J. H. Kim, K. Y. Choi, and K. H. Kim, Appl. Phys. Lett. **108**, 082105 (2016).
[16] A. V. Sanchela, M. Wei, J. H. Lee, G. Kim, H. Jeen, B. Feng, Y. Ikuhara, H. J. Cho, and H. Ohta, e-print arXiv: 1808.07619 (2018).
[17] S. Yu, D. Yoon, and J. Son, Appl. Phys. Lett. **108**, 262101 (2016).
[18] D. Yoon, S. Yu, and J. Son, NPG Asia Mater. **10**, 363 (2018).
[19] J. Wood, M. J. Howes, and D. V. Morgan, Phys. Status Solidi A **74**, 493 (1982).

© Author(s) 2018

[20]J. H. You, J. Q. Lu, and H. T. Johnson, J. Appl. Phys. **99**, 033706 (2006).
[21]N. Miller, E. E. Haller, G. Koblmuller, C. Gallinat, J. S. Speck, W. J. Schaff, M. E. Hawkridge, K. M. Yu, and J. W. Ager, Phys. Rev. B **84**, 075315 (2011).
[22]K. Ganguly, P. Ambwani, P. Xu, J. Seok Jeong, K. Andre Mkhoyan, C. Leighton, and B. Jalan, APL Mater. **3**, 062509 (2015).
[23]K. Ganguly, A. Prakash, B. Jalan, and C. Leighton, APL Mater. **5**, 056102 (2017).
[24]G. Anoop, E. Y. Park, S. Lee, and J. Y. Jo, Electron. Mater. Lett. **11**, 565 (2015).
[25]W. J. Lee, H. J. Kim, J. Kang, D. H. Jang, T. H. Kim, J. H. Lee, and K. H. Kim, Annu. Rev. Mater. Res. **47**, 391 (2017).
[26]D. O. Scanlon, Phys. Rev. B **87**, 161201(R) (2013).
[27]H. M. I. Jaim, S. Lee, X. H. Zhang, and I. Takeuchi, Appl. Phys. Lett. **111**, 172102 (2017).
[28]Q. Z. Liu, J. M. Dai, Y. Zhang, H. Li, B. Li, Z. L. Liu, and W. Wang, J. Alloys Compd. **655**, 389 (2016).
[29]A. V. Sanchela, M. Wei, H. Zensyo, B. Feng, J. Lee, G. Kim, H. Jeen, Y. Ikuhara, and H. Ohta, Appl. Phys. Lett. **112**, 232102 (2018).
[30]A. V. Sanchela, T. Onozato, B. Feng, Y. Ikuhara, and H. Ohta, Phys. Rev. Mater. **1**, 034603 (2017).
[31]D. Chen, F. Niu, L. Qin, S. Wang, N. Zhang, and Y. Huang, Sol. Energy Mater. Sol. Cells **171**, 24 (2017).
[32]N. Zhang, D. Chen, F. Niu, S. Wang, L. Qin, and Y. Huang, Sci. Rep. **6**, 26467 (2016).
[33]B. Hadjarab, A. Bouguelia, and M. Trari, J. Phys. D: Appl. Phys. **40**, 5833 (2007).
[34]E. McCalla, D. Phelan, M. J. Krogstad, B. Dabrowski, and C. Leighton, Phys. Rev. Mater. **2**, 084601 (2018).
[35]U. Klement, U. Erb, A. M. El-Sherik, and K. T. Aust, Mater. Sci. Eng.: A **203**, 177 (1995).
[36]M. G. Kim, U. Dahmen, and A. W. Searcy, J. Am. Ceram. Soc. **70**, 146 (1987).
[37]P. Casey, E. O'Connor, R. Long, B. Brennan, S. A. Krasnikov, D. O'Connell, P. K. Hurley, and G. Hughes, Microelectron. Eng. **86**, 1711 (2009).
[38]J. Green, J. Mater. Sci. **18**, 637 (1983).

© Author(s) 2018